Effective Denoising of InSAR Phase Images via Compressive Sensing

Min-Seok Kang, *Senior Member, IEEE*, and Jae-Min Baek, *Member, IEEE*

***Abstract*—Interferometric synthetic aperture radar (InSAR) denoising is an essential processing step in deformation measurement and topography reconstruction. A noisy InSAR phase image gives rise to the phase unwrapping difficulties and even results in the degradation of various final products of InSAR. To address this issue, we develop a compressive sensing (CS)-based InSAR phase denoising technique in this article. Since the spectrum of the InSAR phase image is usually sparse in the 2-D frequency domain, the estimation of sensing dictionary matrix of the linear system between the InSAR phase signal and its spectrum in the pursuit of sparsity is considered for InSAR phase denoising. The optimization problem derived by the signal parameterization approach is effectively carried out by estimating the basis function that is closely analogous to the strongest signal component in the spectrum of the InSAR phase image. The proposed method is effectively capable of eliminating noise and preserving detailed fringe information of InSAR. In the end, simulations and experimental results demonstrate that the proposed scheme outperforms other conventional InSAR phase denoising methods.**

***Index Terms*—Compressive sensing (CS), interferometric synthetic aperture radar (InSAR), phase filtering, sparse signal processing, synthetic aperture radar (SAR).**

I. Introduction

SYNTHETIC aperture radar (SAR) is an advanced remote sensing technology that utilizes a microwave imaging technique to achieve high-resolution map while taking an advantage of pulse compression and the Doppler effect technology [1], [2], [3], [4], [5], [6]. It has played a significant role in all aspects of the remote sensing applications. One of the important applications in the field of microwave remote sensing is radar interferometry [7], [8], [9]. The interferometric SAR (InSAR) can provide a plenty of information via phase measurements, which enables a variety of capabilities such as topography measurement, vertical surface displacement (uplift or subsidence), lateral surface displacement (velocity), and change detection (via phase decorrelation). The main principle of InSAR technology stems from the basic idea: measuring phase variations by comparing two SAR images acquired from slightly different locations over the same area [10], [11], [12]. Any InSAR measurement has a meaning only if phase values can be unwrapped, i.e., the proper number of cycles is added to the modulo-2π data. However, the presence of noise such as atmospheric effects and phase decorrelation gives rise to the phase unwrapping difficulties and even results in failures in the InSAR process, severely degrading the many final products of InSAR [13], [14], [15]. Therefore, the removal of phase noise should be performed prior to the phase unwrapping, and several algorithms for phase filtering have been studied as an important technology [16], [17], [18], [19], [20], [21], [22], [23], [24], [25].

In [17], the authors developed nonlocal (NL) filter that has attracted substantial attention in the InSAR research community. In contrast to conventional local filters, the NL filter can achieve the phase-noise reduction by measuring a patch resemblance to extract the most proudly concerning components and performing an adaptive mean value obtained using alike pixels. The NL filter is capable of capturing the phase signal with nonconnected pixels, overcoming the limitation of local filtering. In [18], in order to optimize the algorithm for InSAR phase images in a complex formation, authors have implemented enhancements to the NL estimator referenced in [17]. In addition, authors have developed an iterative pyramid method aimed at recovering lost textures from the noise component to maximize texture preservation. However, the computational complexity of a kind of NL filter can be represented as quadratic in the number of adjacent pixels in an image domain, making it particularly expensive to apply directly. In [19], authors presented two novel phase filtering methods based on l_0-norm and l_1-norm regularization within the compressive sensing (CS) framework to reduce phase noise, respectively. More recently, the deep learning technique has improved the performance of InSAR phase denoising. Φ-Net, proposed in [20], utilizes a residual learning scheme that can blindly mitigate phase noise and preserve the details.

Aiming at further improvement of InSAR phase image quality and the shortcomings of existing filtering approaches, we develop an effective CS-based method (CSM) to perform phase-noise reduction in this article. The spectrum of InSAR phase image is sparse in the spatial frequency domain, i.e., it can be represented as a relatively small number of components in some known, possibly orthonormal, basis functions. Based on the sparsity of the spectrum of InSAR phase image, the proposed method focuses on the estimation of the sensing matrix, which can be sparsely represented as the combination of redundant

Manuscript received 2 January 2024; revised 18 April 2024; accepted 7 May 2024. Date of publication 22 May 2024; date of current version 7 October 2024. This work was supported by the Basic Science Research Program through the National Research Foundation of Korea (NRF) funded by the Ministry of Education under Grant 2021R1I1A3043152 and in part by the Research Grant of the Kongju National University in 2023. *(Corresponding author: Jae-Min Baek.)*

Min-Seok Kang is with the Division of Electrical, Electronic, and Control Engineering, Kongju National University, Cheonan 31080, South Korea (e-mail: mskang@kongju.ac.kr).

Jae-Min Baek is with the Department of Mechanical Engineering, Gangneung-Wonju National University, Wonju 26403, South Korea (e-mail: jmbaek@gwnu.ac.kr).

Digital Object Identifier 10.1109/JSTARS.2024.3404048

basis functions, by substituting the phase-noise with the gapped data (GD) in spatial domain. The key idea of the proposed approach is based on the notion that the sensing matrix for InSAR phase image can be perfectly estimated by signal parameterization approach using the basis function that is closely analogous to the strongest signal component in the spectrum of InSAR phase image. The proposed scheme is comprised of two stages: 1) the linear system between the InSAR phase signal and its spectrum is constructed to perform two-dimensional (2-D) CS-based approach and 2) the unknown parameters of basis functions related to the spectrum of InSAR phase signal are estimated from the observed GD dataset using a signal parameterization algorithm based on an orthogonal matching pursuit (OMP)-type basis function-searching scheme. Then, the proposed method can effectively recover InSAR phase signal with high probability, resulting in excellent noise reduction while preserving phase fringes.

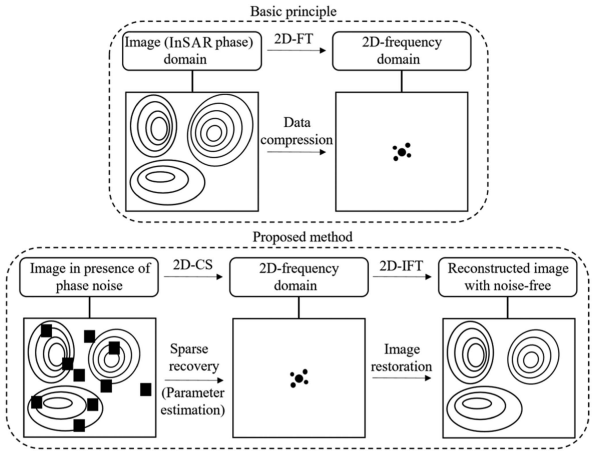

Fig. 1. Conceptual explanations for the 2-D-FT relationship between InSAR phase image and its 2-D-spectrum (top) and the proposed 2-D-CS based method (bottom).

II. Problem and Main Principle Description

A. Characteristic of InSAR Phase Image

The InSAR phase measurements can be utilized as a very sensitive tool to detect and monitor surface deformation phenomena or to retrieve information about the local topography, estimating the digital elevation model of the interest area. However, the phase unwrapping in the InSAR process may result in the low quality of many final products of InSAR, since the phase signal of the InSAR often suffers from some noises such as atmospheric effects and phase decorrelation [26]. Thus, it is necessary for a method to filter off noise signal while preserving the fringe of InSAR phase.

The Fourier transform (FT) is used if one wants to access the geometric characteristics of the spatial domain image [27]. Because the image can be decomposed into its sinusoidal components in the Fourier domain, it is apt to process or examine certain frequencies of the image, thus affecting the geometric structure in the spatial domain. Several general statements can be made about a relationship between the spatial features of an image and frequency components of the FT. It is not intuitively difficult to associate frequencies in the FT with patterns of intensity variations in the image, since the frequency is directly connected to spatial rates of change. This indicates that the common image includes components of all frequencies, but that their amplitude gets smaller for higher frequencies [28]. Hence, low frequencies include more information related to the image than the higher ones. Thus, the 2-D-FT of a signal $f(x, y)$ as an InSAR phase image can be defined via

$$r(u, v) = \int_y \int_x f(x, y) s(u, v) dx dy \tag{1}$$

where

$$f(x, y) = \sum_{i=1}^{L} A_i \delta(x - x_i, y - y_i) \tag{2}$$

$$s(u, v) = \exp(-jux - jvy) \tag{3}$$

where (u, v) represents the spatial frequency domain for (x, y). L denotes the number of sparsely distributed spectral signals $r(u, v)$. After taking 2-D-FT over $f(x, y)$, the spectrum $r(u, v)$ is comprised of sparse signal functions with magnitude A_i with $i = 1, 2, \ldots, L$ centered at the origin in (u, v) domain according to the FT principle mentioned above. In most implementations, the Fourier image of the InSAR phase image is generally shifted in such a way that a sparse representation data including only the slowest varying frequency component is located at $(u = v = 0)$ as shown in Fig. 1. Meanwhile, if the phase noise in the fully-sampled (FS) signal of original InSAR phase image can be considered as a kind of GD (labeled as a black box as shown in Fig. 1) in the image domain, the removal of phase noise can be transformed into the CS reconstruction problem of the spectrum with sparsity. Note that the sparse signal reconstructed using the GD signal based on the 2-D-CS is equivalent to the spectrum of the InSAR phase image using the FS signal based on the 2-D-FT as shown in Fig. 1. Based on this essential idea, we derive a new framework for an InSAR phase reconstruction using CS-based signal parameterization scheme in Section III.

B. Review of CS Theory

The CS theory [29], [30], [31], [32], [33] provides a novel framework for compressing and sampling signals and allows the recovery of a discrete sparse image or signal from the reduced number of samples in comparison with the Nyquist sampling rate. Based on the CS theory, the reconstruction accuracy of sparse signal extremely relies on the sparsity degree of the desired signal and restricted isometry property (RIP) of the sensing matrix [30]. The RIP of the sensing matrix $\mathbf{H}$ can be expressed as

$$(1 - \delta_S) \cdot \|\mathbf{f}\|_2^2 \leq \|\mathbf{H}\mathbf{f}\|_2^2 \leq (1 + \delta_S) \cdot \|\mathbf{f}\|_2^2 \quad \forall \mathbf{f} \tag{4}$$

where $\delta_S \in (0, 1)$ is a small constant related to the sparse signal vector $\mathbf{f}$. $\mathbf{f}$ is said to be an *S–sparse* vector when it has, at most, *S* nonzero elements. Fundamentally, the RIP indicates the incoherence between the *S* column vectors of $\mathbf{H}$ corresponding to the *S* nonzero components, i.e., the submatrix $\mathbf{H}_S$ constructed

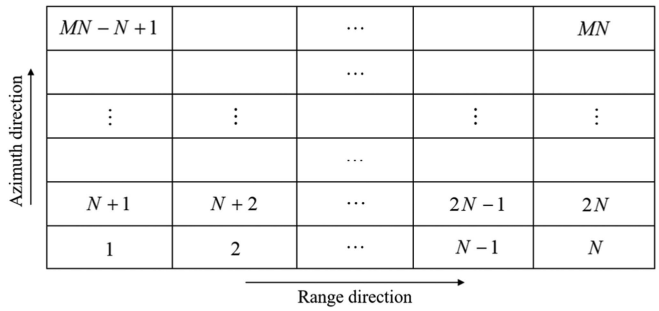

Fig. 2. $M \times N$ grids of matrix domain.

by using the S column vectors of $\mathbf{H}$ has a nearly orthogonality. Actually, the incoherence of $\mathbf{H}$ can be measured by evaluating the spatial distribution of eigenvalues of $\mathbf{H}_S^H \mathbf{H}_S$ [30]. If the statistic of each eigenvalue is tightly bounded around 1, it indicates that $\mathbf{H}$ has a high incoherency. If not, the larger the stochastic deviation of eigenvalues from 1, the less the incoherence of $\mathbf{H}$.

III. Proposed Method

To express the InSAR phase data in the discrete representation, the discrete 2-D-domain can be divided into $M \times N$ grids as depicted in Fig. 2. Then, we can arrange the 2-D grids of the matrix of the InSAR phase data into a vector by row $(1, 2, 3, \ldots, N, N+1, N+2, \ldots, 2N, 2N+1, \ldots, MN)$. (x_i, y_i) is the position of the sparse signal in the grids with the magnitude A_i. We can represent the image of size $M \times N$ as a column vector of the dimension $MN \times 1$ by letting the first M elements of the vector equal the first column of the image, the next M elements equal the second column, and so on. With image formation in this manner, we can represent a broad range of linear processes applied to an image by using the following notation:

$$\mathbf{r} = \mathbf{H}\mathbf{f} \tag{5}$$

where

$$\mathbf{r} = [r(u_1, v_1) \quad r(u_2, v_1) \quad \cdots \quad r(u_n, v_1) \quad r(u_1, v_2) \quad \cdots \quad r(u_n, v_2) \quad \cdots \quad r(u_n, v_m)]^T$$

$$\mathbf{H} = \begin{bmatrix} \mathbf{H}(u_1, v_1, x_1, y_1) & \mathbf{H}(u_1, v_1, x_2, y_2) & \cdots & \mathbf{H}(u_1, v_1, x_L, y_L) \\ \mathbf{H}(u_2, v_1, x_1, y_1) & \mathbf{H}(u_2, v_1, x_2, y_2) & \cdots & \mathbf{H}(u_2, v_1, x_L, y_L) \\ \vdots & \vdots & & \vdots \\ \mathbf{H}(u_n, v_1, x_1, y_1) & \mathbf{H}(u_n, v_1, x_2, y_2) & \cdots & \mathbf{H}(u_n, v_1, x_L, y_L) \\ \mathbf{H}(u_1, v_2, x_1, y_1) & \mathbf{H}(u_1, v_2, x_2, y_2) & \cdots & \mathbf{H}(u_1, v_2, x_L, y_L) \\ \vdots & \vdots & & \vdots \\ \mathbf{H}(u_n, v_2, x_1, y_1) & \mathbf{H}(u_n, v_2, x_2, y_2) & \cdots & \mathbf{H}(u_n, v_2, x_L, y_L) \\ \vdots & \vdots & & \vdots \\ \mathbf{H}(u_n, v_m, x_1, y_1) & \mathbf{H}(u_n, v_m, x_2, y_2) & \cdots & \mathbf{H}(u_n, v_m, x_L, y_L) \end{bmatrix}$$

$$\mathbf{f} = \begin{bmatrix} A_1 & A_2 & \cdots & A_L \end{bmatrix}^T$$

where $\mathbf{f}$ is an $L \times 1$ vector representation by column stacking of an input image, $\mathbf{r}$ is an $MN \times 1$ vector representation by column stacking of a processed image, and $\mathbf{H}$ denotes an $MN \times L$ matrix indicating a linear process applied to the image.

Based on (5), consider the linear system [31], [32], [33]

$$\overline{\mathbf{r}} = \overline{\mathbf{H}}\mathbf{f} \tag{6}$$

where $\overline{\mathbf{r}} = \Psi\mathbf{r}$ and random sampling operation along the vertical direction is implemented by multiplying the random selection identity matrix $\Psi \in \mathbb{C}^{\overline{MN} \times MN}$ on the input data to obtain the GD dataset. $\overline{\mathbf{H}} = \Psi\mathbf{H}$ is a partial dictionary matrix with the size of $\overline{MN} \times L$ provided by original sensing matrix $\mathbf{H}$ with the size of $MN \times L$. The CS theory enables the exact recovery of $\mathbf{f}$ from $\overline{\mathbf{r}}$ with a high probability of success, when the matrix $\overline{\mathbf{H}}$ complies with the RIP by dealing with the following optimization problem constrained by the sparsity of $\mathbf{f}$ [29], [30]:

$$(P_0): \min_{\mathbf{f}} \|\mathbf{f}\|_0 \text{ subject to } \left\|\overline{\mathbf{r}} - \overline{\mathbf{H}}\mathbf{f}\right\|_2 \leq \varepsilon \tag{7}$$

where $\|\cdot\|_2$ represents the l_2-norm of a vector, which means the Euclidean distance. $\|\cdot\|_0$ indicates the l_0-norm of a vector, which means the number of nonzero components in the vector. ε represents an error tolerance as a small positive value. Based on (7), we can restore the desired the spectrum of InSAR phase image by solving an optimization problem using the sparsity constraints of the spectrum in the spatial frequency domain. In this article, the kernel function $s(u, v)$ is expanded as a multivariable quadratic equation based on second-order polynomial coefficients α and β to describe the sparse spectrum of InSAR phase image in detail as follows:

$$s(u, v, \alpha, \beta) \simeq \exp(-jux - ju^2\alpha - jvy - jv^2\beta). \tag{8}$$

Then, the GD signal $r(u_l, v_l)$ can be expressed as

$$r(u_l, v_l) = \sum_{i=1}^{L} A_i' e^{-j(x_i u_i + \alpha_i {u_l}^2 + y_i v_i + \beta_i {v_l}^2)}, \quad l = 1,\ 2,\ \ldots, \overline{MN} \tag{9}$$

where A_i' represents the amplitude of the ith dominant spectrum signal in the spatial frequency domain, l denotes the domain index of the collected $\overline{MN}$ data sequence, and $\overline{MN} < MN$. Then, a signal parameterization approach based on the OMP-type basis function-searching scheme (OBS) is applied to decompose the spectrum of InSAR phase signal into a set of polynomial basis functions. Based on (9), the vector $\overline{\mathbf{r}}$ in (6) can be described as

$$\overline{\mathbf{r}} = \sum_{i=1}^{L} A_i' \left[\overline{\mathbf{h}}(x_i, y_i, \alpha_i, \beta_i)\right] \tag{10}$$

where $\overline{\mathbf{h}}(x_i, y_i, \alpha_i, \beta_i)$ is the basis function vector corresponding to the sparse signal in the ith column vector of $\overline{\mathbf{H}}$, and $\odot$ represents the Hadamard multiplication operator. As the FS-based basis function vector, $\mathbf{h}(x_i, y_i, \alpha_i, \beta_i)$ can be expressed as

$$\mathbf{h}(x_i, y_i, \alpha_i, \beta_i) = \mathbf{l}_x \odot \mathbf{l}_y \odot \mathbf{q}_\alpha \odot \mathbf{q}_\beta \tag{11}$$

where

$$\mathbf{l}_x = \begin{bmatrix} e^{-jx_i u_1} & e^{-jx_i u_2} & \cdots & e^{-jx_i u_{MN}} \end{bmatrix}^T \tag{12}$$

$$\mathbf{l}_y = \begin{bmatrix} e^{-jy_i v_1} & e^{-jy_i v_1} & \cdots & e^{-jy_i v_{MN}} \end{bmatrix}^T \tag{13}$$

$$\mathbf{q}_\alpha = \begin{bmatrix} e^{-j\alpha_i u_1^2} & e^{-j\alpha_i u_2^2} & \cdots & e^{-j\alpha_i u_{MN}^2} \end{bmatrix}^T \tag{14}$$

$$\mathbf{q}_\beta = \left[\; e^{-j\beta_i v_1^2} \quad e^{-j\beta_i v_1^2} \quad \cdots \quad e^{-j\beta_i v_{MN}^2} \;\right]^T. \tag{15}$$

With $k = 1$, let $[\bar{\mathbf{r}}]_1$ denote the vector notation of $r(u_l, v_l)$. Then, $[\bar{\mathbf{r}}]_{k+1}$ can be expressed as

$$[\bar{\mathbf{r}}]_{k+1} = [\bar{\mathbf{r}}]_k - \hat{A}_i' \cdot \bar{\mathbf{h}}(\hat{x}_i, \hat{y}_i, \hat{\alpha}_i, \hat{\beta}_i) \tag{16}$$

and $(\hat{x}_i, \hat{y}_i, \hat{\alpha}_i, \hat{\beta}_i)$ can be obtained using the largest similarity when the Pearson correlation coefficients between a residual signal and the basis function are maximized

$$\left\{(\hat{x}_i, \hat{y}_i, \hat{\alpha}_i, \hat{\beta}_i)\right\} = \underset{(x_i, y_i, \alpha_i, \beta_i)}{\arg\max} \frac{\operatorname{cov}\left(\bar{\mathbf{h}}(x_i, y_i, \alpha_i, \beta_i), [\bar{\mathbf{r}}]_k\right)}{\sigma_{\bar{\mathbf{h}}}\sigma_{\bar{\mathbf{r}}}} \tag{17}$$

where $\operatorname{cov}(\bar{\mathbf{h}}(x_i, y_i, \alpha_i, \beta_i), [\bar{\mathbf{r}}]_k) = \mathrm{E}[(\bar{\mathbf{h}}(x_i, y_i, \alpha_i, \beta_i) - \mu_{\bar{\mathbf{h}}})([\bar{\mathbf{r}}]_k - \mu_{\bar{\mathbf{r}}})]$, $\sigma_{\bar{\mathbf{h}}}$ and $\sigma_{\bar{\mathbf{r}}}$ are the standard deviations of $\bar{\mathbf{h}}(x_i, y_i, \alpha_i, \beta_i)$ and $[\bar{\mathbf{r}}]_k$, respectively. $\mathrm{E}[\cdot]$ is the expectation operator. $\mu_{\bar{\mathbf{h}}}$ and $\mu_{\bar{\mathbf{r}}}$ are the mean vectors of $\bar{\mathbf{h}}(x_i, y_i, \alpha_i, \beta_i)$ and $[\bar{\mathbf{r}}]_k$, respectively. The basis function vector that bears a great resemblance to the strongest signal component in $\bar{\mathbf{h}}$ can be estimated as $\bar{\mathbf{h}}(\hat{x}_i, \hat{y}_i, \hat{\alpha}_i, \hat{\beta}_i)$ corresponding to the sparse signal in the ith column vector of $\bar{\mathbf{H}}$. It was proven that an energy of $[\bar{\mathbf{r}}]_{k+1}$ in (16) tends to converge to zero as k approaches infinity [30]. Thus, the operations of (16) and (17) are repetitively carried out until the total energy of $[\bar{\mathbf{r}}]_{k+1}$ is less than a predetermined limit.

Then, the orthogonal projection on the residual signal is carried out to find the magnitude $\hat{A}_i'$, calculating the following least-square solution:

$$\hat{A}_i' = (\hat{\bar{\mathbf{h}}}^H \hat{\bar{\mathbf{h}}})^{-1} \hat{\bar{\mathbf{h}}}^H \bar{\mathbf{r}} \tag{18}$$

where $\hat{\bar{\mathbf{h}}} = \hat{\bar{\mathbf{l}}}_x \odot \hat{\bar{\mathbf{l}}}_y \odot \hat{\bar{\mathbf{q}}}_\alpha \odot \hat{\bar{\mathbf{q}}}_\beta$, denotes an $\overline{MN} \times 1$ element basis function vector that is constructed by the estimated parameters $(\hat{x}_i, \hat{y}_i, \hat{\alpha}_i, \hat{\beta}_i)$. In general, the iteration number of OMP relies on signal sparsity [30]. In order to terminate the iteration procedure from (16)–(18), the cost function C_1 as a stopping criterion can be designed by

$$C_1 = \left\|[\bar{\mathbf{r}}]_{k+1} - [\bar{\mathbf{r}}]_k\right\|_2^2 \Big/ \left\|[\bar{\mathbf{r}}]_k\right\|_2^2 < \eta \tag{19}$$

where $[\bar{\mathbf{r}}]_k$ indicates the kth iterative residual, $0 < \eta < 1$ represents the iterative termination threshold. In this article, we selected $\eta = 0.1$ as the stopping criterion for iterations in all experimental trials. When the energy of adjacent residual signal difference is less than the predetermined threshold η, the sparse representation of the spectrum of InSAR phase signal can be accurately estimated by the OBS. If the exact basis function estimation is successfully carried out, the dictionary $\hat{\mathbf{H}}$ can be formed as the $MN \times \hat{L}$ matrix based on $\hat{L}$ basis function vectors with the FS-based $\hat{\mathbf{h}}(\hat{x}_i, \hat{y}_i, \hat{\alpha}_i, \hat{\beta}_i) \in \mathbb{C}^{MN \times 1}$

$$\hat{\mathbf{H}} = \Big[\hat{\mathbf{h}}(\hat{x}_1, \hat{y}_1, \hat{\alpha}_1, \hat{\beta}_1) \quad \hat{\mathbf{h}}(\hat{x}_2, \hat{y}_2, \hat{\alpha}_2, \hat{\beta}_2) \quad \cdots \quad \hat{\mathbf{h}}(\hat{x}_{\hat{L}}, \hat{y}_{\hat{L}}, \hat{\alpha}_{\hat{L}}, \hat{\beta}_{\hat{L}})\Big] \tag{20}$$

where $\hat{L}$ is the estimated number of sparse target signals.

Based on the descriptions found in (6)–(18), all of the steps required to restore the sensing matrix of (20) are iteratively carried out until the stopping criterion C_1 between the kth and $(k+1)$th iterations is satisfied with the terminating rule according to (19). Then, the denoised InSAR phase data in the spatial domain can be reconstructed by using the parameters $\{(\hat{x}_i, \hat{y}_i, \hat{\alpha}_i, \hat{\beta}_i, \hat{A}_i')\}_{i=1}^{\hat{L}}$ estimated from the sparse spectrum in the 2-D-frequency domain as follows:

$$\hat{r}(u_l, v_l) = \sum_{i=1}^{\hat{L}} \hat{A}_i' e^{-j(\hat{x}_i u_i + \hat{\alpha}_i u_l{}^2 + \hat{y}_i v_i + \hat{\beta}_i v_l{}^2)}, \quad l = 1, 2, \ldots, MN. \tag{21}$$

Note that the restored signal in (21) has an FS signal set of sequence data in contrast to the GD data in (9).

From the mathematical derivations in (5)–(21), Fig. 3 illustrates the detailed process of the proposed scheme.

Procedure of the proposed scheme

- **Initialization**: Construct $\mathbf{f}$ and $\mathbf{r}$ as the vector representation by column stacking.
- **Main iteration**: Increment k by 1 and implement the following stages until the stopping criterion is satisfied:

Step 1: Estimate the parameters $(x_i, y_i, \alpha_i, \beta_i)$ based on the similarity between basis functions and residue as

$$\left\{(\hat{x}_i, \hat{y}_i, \hat{\alpha}_i, \hat{\beta}_i)\right\} = \underset{(x_i, y_i, \alpha_i, \beta_i)}{\arg\max} \frac{\operatorname{cov}\left(\bar{\mathbf{h}}(x_i, y_i, \alpha_i, \beta_i)\,,\, [\bar{\mathbf{r}}]_k\right)}{\sigma_{\bar{\mathbf{h}}}\sigma_{\bar{\mathbf{r}}}}.$$

Step 2: Calculate the amplitude $\hat{A}_i'$ using the basis functions $\hat{\mathbf{h}} = \hat{\mathbf{l}}_x \odot \hat{\mathbf{l}}_y \odot \hat{\mathbf{q}}_\alpha \odot \hat{\mathbf{q}}_\beta$ chosen so far as follows:

$$\hat{A}_i' = (\hat{\mathbf{h}}^H \hat{\mathbf{h}})^{-1} \hat{\mathbf{h}}^H \bar{\mathbf{r}}.$$

Step 3: Calculate the residual $[\bar{\mathbf{r}}]_{k+1}$ as follows:

$$[\bar{\mathbf{r}}]_{k+1} = [\bar{\mathbf{r}}]_k - \hat{A}_i' \cdot \bar{\mathbf{h}}(\hat{x}_i, \hat{y}_i, \hat{\alpha}_i, \hat{\beta}_i).$$

Step 4: Check the relative change of the cost function C_1

$$C_1 = \left\|[\bar{\mathbf{r}}]_{k+1} - [\bar{\mathbf{r}}]_k\right\|_2^2 \Big/ \left\|[\bar{\mathbf{r}}]_k\right\|_2^2 < \eta.$$

- **Output**: The denoised-InSAR phase image can be generated by the reconstructed signal (21), after estimating $\left\{(\hat{x}_i, \hat{y}_i, \hat{\alpha}_i, \hat{\beta}_i, \hat{A}_i')\right\}_{i=1}^{\hat{L}}$ satisfying (17) and (18).

Fig. 3. Typical flowchart illustrating stages of the proposed scheme.

IV. Results and Analysis

Several tests are performed to verify the effectiveness and robustness of the proposed phase denoising method using both simulated and real InSAR phase. The NL filter [17], a pyramidal representation based NL filter (PNL) [18], CSM [19], and Φ-Net [20] are used for comparison in this section.

A. Simulation Results

Initially, we performed simulations to prove the robustness of the proposed approach and evaluate its filtering performance. All the results were obtained from the MATLAB R2021a code 10 on an AMD Ryzen 9 5900X 12-Core Processor at 3.70 GHz-CPU. First, we constructed the unwrapped phase data to simulate the

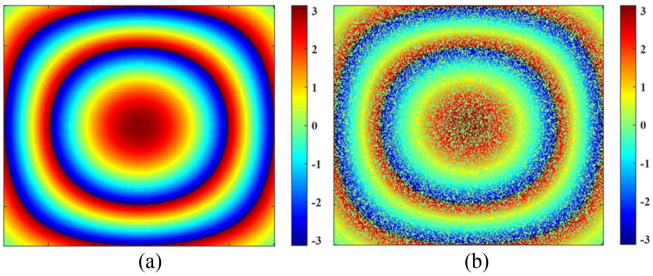

Fig. 4. Simulated interferometric phase data. (a) Simulated wrapped phase data. (b) GD data of (a).

basic characteristics of the interferometric fringe in nature. Then, we can obtain the simulated wrapped InSAR phase image in a complex formation as shown in Fig. 4(a). The contamination of the InSAR phase image was implemented by the some noise patterns occurring globally across entire regions. Meanwhile, all of the positions belonging to the noisy data in InSAR phase were eliminated to yield the GD dataset for the proposed method as shown in Fig. 4(b).

The simulations were implemented to compare the performance of the NL filter method [17], PNL filter method [18], CSM [19], Φ-Net [20], and the proposed method. The NL and PNL filter estimators were applied with a search window of size $|W| = 21 \times 21$ and a similarity window of size $|\Delta| = 7 \times 7$, respectively. According to the simulation results, one can see that all the methods yield somewhat improvement in the elimination of the noise in InSAR phase images as shown in Fig. 5(a)–(d), and (f). However, compared to the original InSAR phase image [see Fig. 4(a)], it is observed that some specific regions between discontinuous fringes affect the difficulty of the noise filtering in the NL method [see Fig. 5(a)]. In PNL filtering, we can observe that noise filtering of the PNL method fails the recovery of the detail fringes of the InSAR image in some noise-dense regions as shown in Fig. 5(b). Fig. 5(c) demonstrates that the CSM alternatively updates the dictionary matrix and sparse parameter vector for each subproblem within the CS framework to reduce phase noise. Fig. 5(d) shows the Φ-Net method can also achieve good performance, which is almost analogous to that of the CSM. On the other hand, one can see that the resulting InSAR phase image restored by the proposed method, as depicted in Fig. 5(f), has noticeable visual improvement compared with the other four methods. The accurate parameter estimation based on the sparse spectrum [see Fig. 5(e)] of InSAR phase image was made possible by using the OBS based on similarity maximization between the basis function and the residual. The sparsity of the spectrum of InSAR phase image helps to achieve a better filtering performance, since more details of fringes can be fully described by the CS-based signal parameterization scheme.

Fig. 6 illustrates the phase unwrapping results of Fig. 5 obtained by the NL filter method, PNL filter method, CSM, Φ-Net, and the proposed method. In order to analyze the quantitative evaluation of the filtering performance, each unwrapped phase image was compared with the reference unwrapped phase [see Fig. 6(a)] by using the performance evaluation function, i.e.,

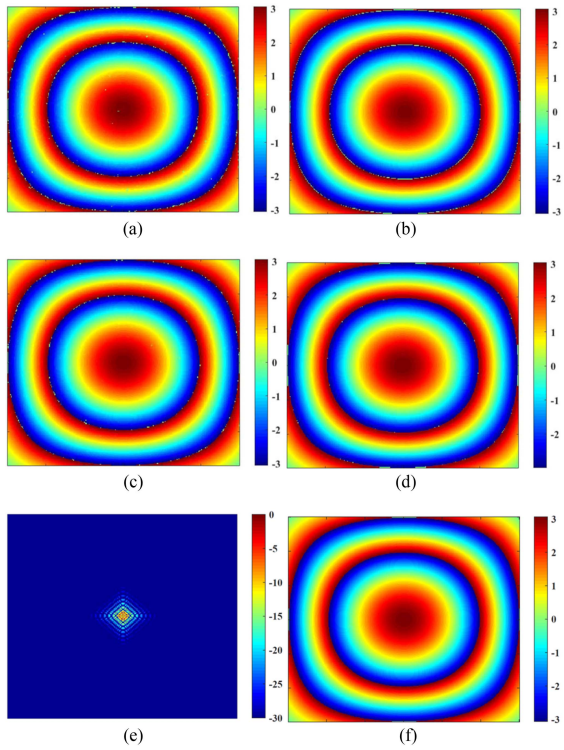

Fig. 5. Simulation results for performance analysis using simulated interferometric phase data. (a) InSAR phase restored by the NL filter from GD data. (b) InSAR phase restored by the PNL filter from GD data. (c) InSAR phase restored by the CSM from GD data. (d) InSAR phase restored by the Φ-Net from GD data. (e) Spectrum of InSAR phase reconstructed by the proposed method from GD data (dB scale). (f) InSAR phase restored by the proposed method from GD data.

TABLE I
SIMULATION RESULTS

	NL	PNL	CSM	Φ-Net	Proposed
RMSE	0.1963	0.1845	0.1655	0.1538	0.1377
SSIM	0.832	0.874	0.895	0.918	0.934

the root mean square error (RMSE) and the structural similarity index measure (SSIM). The RMSE can be employed as a measure of the agreement or precision based on the difference between the filtered and original InSAR phase. The smaller RMSE indicates that the filtered InSAR phase image is closer to the original one, but the correlation between pixels in images is not considered in RMSE. Thus, the SSIM is used for measuring the structural similarity between the filtered and original InSAR phase images. A higher SSIM indicates that the structural similarity of information is maintained better during the denoising process. The detailed simulation results for the evaluation metric are described in Table I. One can see that the RMSE obtained by the proposed method is considerably lower than those of four different methods, which reveals that the detail preservation of fringes and capacity of noise suppression of the proposed method are substantially better. One can see that the proposed approach achieves the highest SSIM, which indicates that most phase-noise are filtered out by the proposed method with the detailed fringe information among the five schemes.

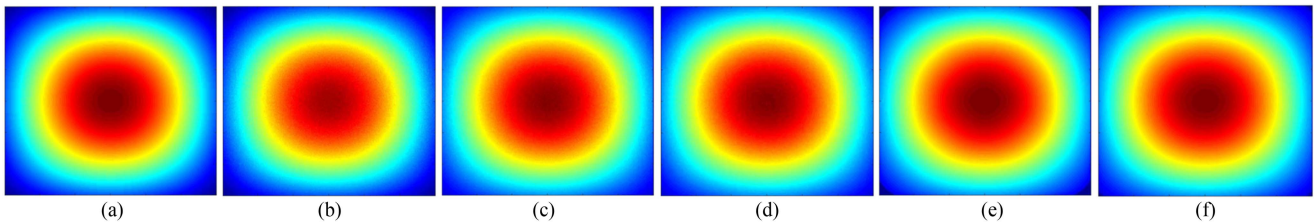

Fig. 6. Comparison of recovered phase unwrapping results from five different algorithms using the simulated InSAR phase image. (a) Ground truth. (b) Phase unwrapping result restored by NL filter. (c) Phase unwrapping result restored by PNL filter. (d) Phase unwrapping result restored by CSM. (e) Phase unwrapping result restored by Φ-Net. (f) Phase unwrapping result restored by the proposed method.

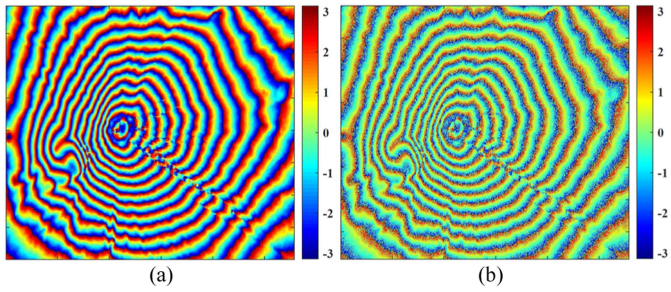

Fig. 7. Real measured InSAR phase image and noised data. (a) Real measured InSAR phase data. (b) GD data of (a).

Consequently, we conclude that the proposed method is capable of offering better robustness against phase-noise than the conventional approaches. Furthermore, it is observed that it is more suitable for the preservation of phase fringes in the high level of added noise regions.

B. Experimental Results With Real Measured Data

The interferometric phase of real measured SAR data, namely, the public release data of Earth remote sensing [9], provided by the German Aerospace Center and the European Space Agency, was used to analyze the evaluation of the filtering performance via the proposed method as depicted in Fig. 7(a). The dataset has been artificially contaminated under the some noise conditions according to a specific coherence pattern. In the same manner as mentioned in Section IV-A, the GD dataset was constructed from the FS dataset of the original InSAR phase image as shown in Fig. 7(b). Then, we compare the proposed method with four widely used methods to analyze the filtering performance of the proposed scheme: NL filter, PNL filter, CSM, and Φ-Net. It can be observed that all the methods provide some apparent filtering performance of phase-noise in InSAR phase images as depicted in Fig. 8(a)–(d), and (f). The result of the NL method needs further improvement in the filtering quality; the residual phase-noise of the filtered version was slightly dispersed in some noise-dense region, which consequently yields some poor visual quality of the InSAR phase image as displayed in Fig. 8(a). One can see that the outcome of the PNL filter in some fringe dense region results in the preservation difficulty of fringe details to some degree due to the influence of phase-noise as given in Fig. 8(b). From the results displayed in Fig. 8(c), the presence of some noise lingering around the highest area is

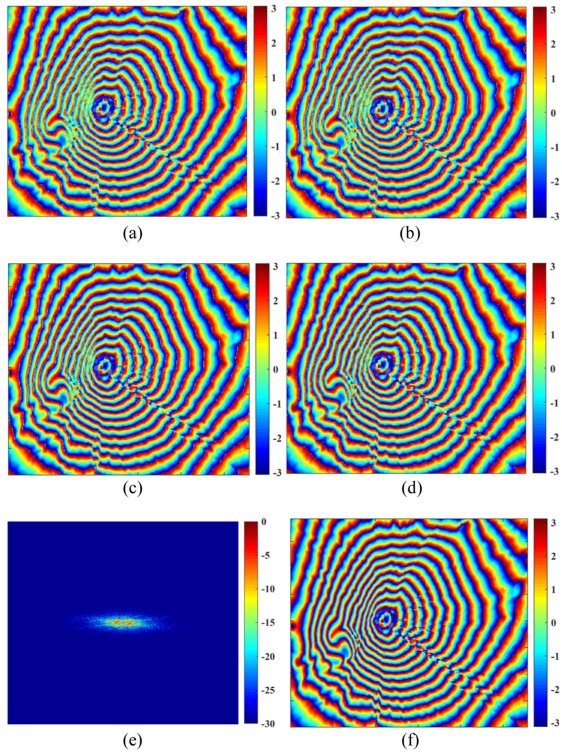

Fig. 8. Experimental results for performance analysis using real data. (a) InSAR phase restored by the NL filter from GD data. (b) InSAR phase restored by the PNL filter from GD data. (c) InSAR phase restored by the CSM from GD data. (d) InSAR phase restored by the Φ-Net from GD data. (e) Spectrum of InSAR phase reconstructed by the proposed method from GD data (dB scale). (f) InSAR phase restored by the proposed method from GD data.

clearly observed in the InSAR phase image although most of the noise has been removed by the CSM. It can be observed in Fig. 8(d) that the Φ-Net yields slightly some visual improvement on the InSAR phase image compared with that of the CSM for the entire area of the InSAR phase image. Meanwhile, in the proposed method, the spectrum of the InSAR phase image, obtained by the estimation of sensing matrix based on the OBS with polynomial basis functions, is sparsely represented using a relatively small number of components in the spatial frequency domain [see Fig. 8(e)]. Owing to the sparsity of spectrum, one can see that the proposed scheme achieved excellent creation of a high-quality InSAR phase image with well-preserved fringe detail by eliminating optimally the phase noise, as depicted in Fig. 8(f).

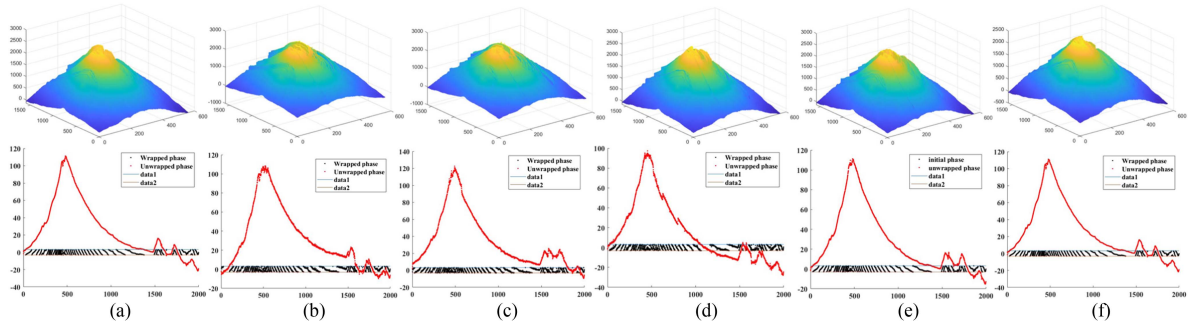

Fig. 9. Comparison of recovered phase unwrapping results (first row) and cross-sectional view of phase unwrapping results (second row) from five different algorithms using the real measured InSAR phase image. (a) Ground truth. (b) Phase unwrapping result restored by NL filter. (c) Phase unwrapping result restored by PNL filter. (d) Phase unwrapping result restored by CSM. (e) Phase unwrapping result restored by Φ-Net. (f) Phase unwrapping result restored by the proposed method.

TABLE II
EXPERIMENTAL RESULTS

	NL	PNL	CSM	Φ-Net	Proposed
RMSE	0.2264	0.2180	0.2002	0.1987	0.1821
SSIM	0.854	0.862	0.884	0.907	0.918

Fig. 9 presents the results of phase unwrapping through the five different denoising methods. From phase unwrapping results shown in Fig. 9(b)–(e), it is observed that there are obvious phase jumps between the two sides of the shadow area due to a few discontinuities. Meanwhile, it can be easily recognized that the phase unwrapping result obtained by the proposed method shown in Fig. 9(f) was nearly a match for the reference unwrapped phase given in Fig. 9(a). Thus, we infer that the proposed method is superior to other denoising methods since it not only filters more amount of noise but also maintains the fringe completeness effectively. To further evaluate the restoration accuracy of each method, we obtained both RMSE and SSIM of the phase difference between the phase unwrapping results of five different methods and the reference unwrapped phase [see Fig. 9(a)]. The detailed experimental results to examine the quantitative evaluation of the filtering performance are summarized in Table II. As expected, the outcome of the InSAR phase image obtained using the proposed scheme was the best among five different methods in terms of the quantitative evaluation of the filtering performance of both RMSE and SSIM. Thus, we infer that the proposed method can effectively assess the phase unwrapping result qualitatively and quantitatively.

Finally, all the experimental results proved that the proposed scheme is most suitable for InSAR phase denoising in comparison with the four different methods considered in this study.

V. DISCUSSION

Since the InSAR measurements are typically acquired through observations of extensive geographical areas, the spectrum of InSAR phase image is sparse in the spatial frequency domain, i.e., it can be represented as a relatively small number of components. The linear system between the InSAR phase signal and its spectrum is constructed to perform a 2-D CS-based approach and the unknown parameters of basis functions related to the spectrum of the InSAR phase signal are estimated from the observed GD dataset using a signal parameterization algorithm based on the OBS. Then, the proposed method can effectively recover the InSAR phase signal with high probability, resulting in excellent noise reduction while preserving phase fringes. Besides randomly distributed noise signals within the InSAR phase image, specific noise patterns occurring locally in certain areas can also be addressed by the CS-based InSAR phase denoising technique.

Another important issue in the proposed method for denoising InSAR phase images is determining the appropriate step size, i.e., the number of samples in the search ranges of the candidate parameters. If the range of the estimated variables is subdivided into smaller intervals, the restored sparse spectrum will be estimated more accurately. However, it comes with the drawback of the increased computational complexity of the algorithm.

VI. CONCLUSION

This article presents a novel approach for CS-based InSAR phase denoising. The frequencies associated in the FT with patterns of intensity variations in an InSAR phase image are usually sparse in the spectrum domain. Due to the sparse spectrum of InSAR phase image, a signal parameterization scheme based on the OBS approach from the observed GD dataset can be applied to decompose the InSAR phase signal into a set of polynomial basis functions. Then, all of the steps required to recover the sensing matrix of linear system between the InSAR phase signal and its spectrum are iteratively carried out to precisely retrieve the InSAR phase signal while preserving the spatial resolution. The principles of the proposed approach were fully described in this article. The proposed method for InSAR denoising is capable of achieving remarkable good preservation of fringe details and noise cancellation. The simulation and experimental results validated a considerable improvement in performance on the aspects of noise reduction quality and efficiency in comparison to conventional InSAR denoising methods.

REFERENCES

[1] G. Krieger et al., "TanDEM-X: A satellite formation for high resolution SAR interferometry," *IEEE Trans. Geosci. Remote Sens.*, vol. 45, no. 11, pp. 3317–3341, Nov. 2007, doi: 10.1109/TGRS.2007.900693.

[2] J. S. Lee, K. W. Hoppel, S. A. Mango, and A. R. Miller, "Intensity and phase statistics of multilook polarimetric and interferometric SAR imagery," *IEEE Trans. Geosci. Remote Sens.*, vol. 32, no. 5, pp. 1017–1028, Sep. 1994.

[3] R. Lanari et al., "Generation of digital elevation models by using SIR-C/X-SAR multifrequency two-pass interferometry: The Etna case study," *IEEE Trans. Geosci. Remote Sens.*, vol. 34, no. 5, pp. 1097–1113, Sep. 1996, doi: 10.1109/36.536526.

[4] R. Bamler and P. Hartl, "Synthetic aperture radar interferometry," *Inverse Probl.*, vol. 14, no. 4, pp. R1–R54, Aug. 1998, doi: 10.1088/0266-5611/14/4/001.

[5] H. A. Zebker and J. Villasenor, "Decorrelation in interferometric radar echoes," *IEEE Trans. Geosci. Remote Sens.*, vol. 30, no. 5, pp. 950–959, Sep. 1992, doi: 10.1109/36.175330.

[6] M. S. Kang, J. H. Bae, S. H. Lee, and K. T. Kim, "Bistatic ISAR imaging and scaling of highly maneuvering target with complex motion via compressive sensing," *IEEE Trans. Aerosp. Electron. Syst.*, vol. 54, no. 6, pp. 2809–2826, Dec. 2018.

[7] X. Lin, F. Li, D. Meng, D. Hu, and C. Ding, "Nonlocal SAR interferometric phase filtering through higher order singular value decomposition," *IEEE Geosci. Remote Sens. Lett.*, vol. 12, no. 4, pp. 806–810, Apr. 2015.

[8] G. Baier, C. Rossi, M. Lachaise, X. X. Zhu, and R. Bamler, "A nonlocal InSAR filter for high-resolution DEM generation from TanDEM-X interferograms," *IEEE Trans. Geosci. Remote Sens.*, vol. 56, no. 11, pp. 6469–6483, Nov. 2018, doi: 10.1109/TGRS.2018.2839027.

[9] M. S. Kang and K. T. Kim, "Automatic SAR image registration via Tsallis entropy and iterative search process," *IEEE Sensors J.*, vol. 20, no. 14, pp. 7711–7720, Jul. 2020.

[10] J. Moreira et al., "X-SAR interferometry: First results," *IEEE Trans. Geosci. Remote Sens.*, vol. 33, no. 4, pp. 950–956, Jul. 1995, doi: 10.1109/36.406681.

[11] D. Masonnet et al., "The displacement field of the Landers earthquake mapped by radar interferometry," *Nature*, vol. 364, no. 6433, pp. 138–142, Jul. 1993.

[12] D. Massonnet, P. Briole, and A. Arnaud, "Deflation of Mount Etna monitored by spaceborne radar interferometry," *Nature*, vol. 375, no. 6532, pp. 567–570, Jun. 1995, doi: 10.1038/375567a0.

[13] D. C. Ghiglia and M. D. Pritt, *Two-Dimensional Phase Unwrapping: Theory, Algorithms, and Software*. New York, NY, USA: Wiley, 1998.

[14] J. S. Lee, K. P. Papathanassiou, T. L. Ainsworth, M. R. Grunes, and A. Reigber, "A new technique for noise filtering of SAR interferometric phase images," *IEEE Trans. Geosci. Remote Sens.*, vol. 36, no. 5, pp. 1456–1465, Sep. 1998.

[15] C. F. Chao, K. S. Chen, and J. S. Lee, "Refined filtering of interferometric phase from InSAR data," *IEEE Trans. Geosci. Remote Sens.*, vol. 51, no. 12, pp. 5315–5323, Dec. 2013, doi: 10.1109/TGRS.2012.2234467.

[16] M. S. Seymour and I. G. Cumming, "Maximum likelihood estimation for SAR interferometry," in *Proc. IEEE Int. Geosci. Remote Sens. Symp.*, 1994, pp. 2272–2275, doi: 10.1109/IGARSS.1994.399711.

[17] C. A. Deledalle, L. Denis, and F. Tupin, "NL-InSAR: Nonlocal interferogram estimation," *IEEE Trans. Geosci. Remote Sens.*, vol. 49, no. 4, pp. 1441–1452, Apr. 2011, doi: 10.1109/TGRS.2010.2076376.

[18] R. Chen, W. Yu, R. Wang, G. Liu, and Y. Shao, "Interferometric phase denoising by pyramid nonlocal means filter," *IEEE Geosci. Remote Sens. Lett.*, vol. 10, no. 4, pp. 826–830, Jul. 2013.

[19] X. Luo, X. Wang, Y. Wang, and S. Zhu, "Efficient InSAR phase noise reduction via compressive sensing in the complex domain," *IEEE J. Sel. Topics Appl. Earth Observ. Remote Sens.*, vol. 11, no. 5, pp. 1615–1632, May 2018.

[20] F. Sica, G. Gobbi, P. Rizzoli, and L. Bruzzone, "Φ-Net: Deep residual learning for InSAR parameters estimation," *IEEE Trans. Geosci. Remote Sens.*, vol. 59, no. 5, pp. 3917–3941, May 2021.

[21] N. Wu, D. Z. Feng, and J. Li, "A locally adaptive filter of interferometric phase images," *IEEE Geosci. Remote Sens. Lett.*, vol. 3, no. 1, pp. 73–77, Jan. 2006, doi: 10.1109/LGRS.2005.856703.

[22] A. L. B. Candeias, J. C. Mura, L. V. Dutra, J. R. Moreira, and P. P. Santos, "Interferogram phase noise reduction using morphological and modified median filters," in *Proc. 1995 IEEE Int. Geosci. Remote Sens. Symp.*, 1995, pp. 166–168, doi: 10.1109/IGARSS.1995.519679.

[23] W. B. Abdallah and R. Abdelfattah, "An enhanced weighted median filter for noise reduction in SAR interferograms," in *Proc. Int. Conf. Adv. Concepts Intell. Vis. Syst.*, 2013, pp. 49–59.

[24] D. Meng, V. Sethu, E. Ambikairajah, and L. Ge, "A novel technique for noise reduction in InSAR images," *IEEE Geosci. Remote Sens. Lett.*, vol. 4, no. 2, pp. 226–230, Apr. 2007, doi: 10.1109/LGRS.2006.888845.

[25] J. Xue, K. Deng, and F. Zhu, "Gauss weighted periodic pivoting filtering algorithm for InSAR interferogram," *Sci. Surv. Mapp.*, vol. 3, pp. 40–45, Mar. 2011.

[26] R. Goldstein, H. A. Zebker, and C. L. Werner, "Satellite radar interferometry: Two-dimensional phase unwrapping," *Radio Sci.*, vol. 23, no. 4, pp. 713–720, Jul./Aug. 1988, doi: 10.1029/RS023i004p00713.

[27] V. C. Chen and H. Ling, *Time-Frequency Transforms for Radar Imaging and Signal Analysis*. Boston, MA, USA: Artech House, 1995.

[28] R. C. Gonzalez and R. E. Woods, *Digital Image Processing*, II ed. New Delhi, India: Pearson Education, 2005.

[29] D. L. Donoho, "Compressive sensing," *IEEE Trans. Inf. Theory*, vol. 52, no. 4, pp. 1289–1306, 2006.

[30] M. Elad, *Sparse and Redundant Representations*. Berlin, Germany: Springer, 2010.

[31] M. S. Kang and J. M. Baek, "SAR image reconstruction via incremental imaging with compressive sensing," *IEEE Trans. Aerosp. Electron. Syst.*, vol. 59, no. 4, pp. 4450–4463, Aug. 2023, doi: 10.1109/TAES.2023.3241893.

[32] G. Xu, B. Zhang, H. Yu, J. Chen, M. Xing, and W. Hong, "Sparse synthetic aperture radar imaging from compressed sensing and machine learning: Theories, applications and trends," *IEEE Geosci. Remote Sens. Mag.*, vol. 10, no. 4, pp. 32–69, Dec. 2022, doi: 10.1109/MGRS.2022.3218801.

[33] M. S. Kang, S. J. Lee, S. H. Lee, and K. T. Kim, "ISAR imaging of High-Speed maneuvering target using gapped Stepped-Frequency waveform and compressive sensing," *IEEE Trans. Image. Process.*, vol. 26, no. 10, pp. 5043–5056, Oct. 2017.

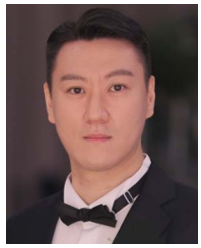

Min-Seok Kang (Senior Member, IEEE) received the B.S. (*summa cum laude*) degree in electrical and computer engineering from Ajou University, Suwon, South Korea, in 2013, and the M.S. and Ph.D. degrees in electrical engineering from Pohang University of Science and Technology (POSTECH), Pohang, South Korea, in 2015 and 2019, respectively.

From 2019 to 2020, he was a Senior Researcher with Agency for Defense Development, Daejeon, South Korea. Since 2020, he has been with the Division of Electrical, Electronic, and Control Engineering, Kongju National University, Cheonan, South Korea, where he is currently an Assistant Professor. His current research interests include radar signal processing, synthetic aperture radar (SAR) and inverse SAR imaging, interferometric SAR processing, array pattern synthesis, compressive sensing and artificial intelligence algorithms for radar signal processing, optimization theory, and control theory.

Dr. Kang was the recipient of a National Scholarship for Natural Science and Engineering from Korea Student Aid Foundation in 2007, a Yonam scholarship from LG Yonam Foundation in 2015, and the Outstanding Doctoral Dissertation Award from the POSTECH in 2019.

Jae-Min Baek (Member, IEEE) received the B.S. degree in mechanical engineering from Korea University, Seoul, South Korea, in 2012, and the Ph.D. degree (M.S.-Ph.D. joint program) in IT engineering from Pohang University of Science and Technology (POSTECH), Pohang, South Korea, in 2018.

From 2018 to 2020, he was with the Agency for Defense Development, Daejeon, South Korea. Since 2020, he has been with the Department of Mechanical Engineering, Gangneung-Wonju National University, Wonju, South Korea. His main research interests include control theory, adaptive/robust control, robotics, mechatronics, and synthetic aperture radar processing.